Ordered multimodal porous carbon with hierarchical nanostructure as high performance electrode material for supercapacitor

Journal:	*RSC Advances*
Manuscript ID:	RA-ART-07-2014-006724.R1
Article Type:	Paper
Date Submitted by the Author:	07-Aug-2014
Complete List of Authors:	Chaudhari, Sudeshna; Korea University, Advanced Materials Chemistry Kwon, Seon Young; Korea University, Advanced Materials Chemistry Yu, Jong-Sung; Korea University, Advanced Materials Chemistry

Table of Content-

Unique hierarchical nanostructure of OMPC facilitates fast mass transport along with large surface area for electrical charge storage.

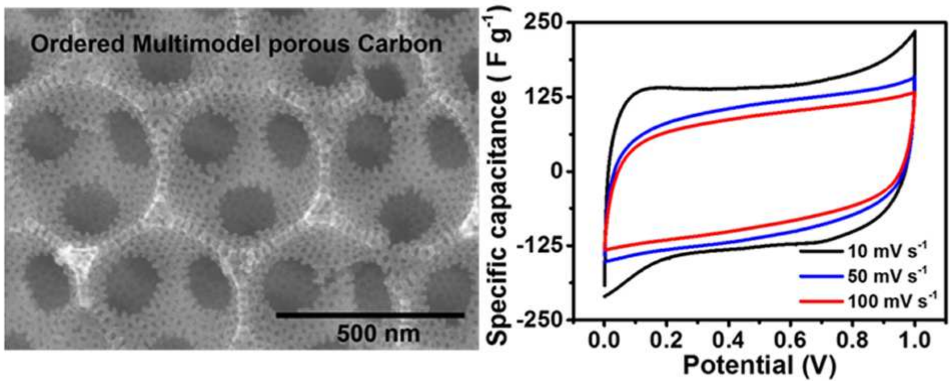

Ordered multimodal porous carbon with hierarchical nanostructure as high performance electrode material for supercapacitor

Sudeshna Chaudhari, Seon Young Kwon and Jong-Sung Yu*

Received (in XXX, XXX) Xth XXXXXXXXX 20XX, Accepted Xth XXXXXXXXX 20XX
DOI: 10.1039/b000000x

Ordered multimodal porous carbon (OMPC) with hierarchical nanostructure is successfully synthesized by using a hard template method. Scanning electron microscopy (SEM), transmission electron microscopy (TEM) and Brunauer-Emmett-Teller (BET) analyses are employed to characterize the as-synthesized OMPC sample. Based on the characterization results, it is confirmed that the as-prepared sample has multimodal porous structure with unique structural characteristics, such as high surface area (1161 m^2 g^{-1}) and well-developed three-dimensional (3D) interconnected ordered macropore framework with open mesopores embedded in the macropore walls, which enable the OMPC to effectively store and release large electrical charges. The electrochemical performance reveals that the combined hierachical meso- and macroporosity of OMPC electrode plays an important role in improving cycle stability and rate performance of the electrode. The OMPC electrode exhibits a highest specific capacitance of 257 F g^{-1} at low current density of 0.5 A g^{-1} and 152 F g^{-1} at high current density of 10 A g^{-1} in aqueous electrolyte of 1.0 M H_2SO_4. This hierarchical nanostructure of OMPC can deliver energy density of 8.4 Wh kg^{-1} at a power density of 5.0 kW kg^{-1}. The specific capacitance of about 90% is preserved after 1200 cycles, revealing excellent cycling stability of OMPC. Such excellent performance is attributed to the unique hierarchical nanostructure of the OMPC, which facilitates fast mass transport along with large surface area for high electrical charge storage compared to commonly used electrode material such as activated carbon (AC).

1. Introduction

Increasing demand for high-power applications such as electric vehicles has triggered significant research efforts in the design and development of novel electrode materials for advanced energy storage devices. Electrochemcial capacitor (ECs) (also known as supercapacitor) as an important next generation energy storage device, has received extensive attention, mainly due to its higher power density than batteries and higher energy density than conventional capacitors.[1,2] Electrochemical capacitors can be classified as electric double-layer capacitors (EDLCs) and pseudocapacitors. In EDLCs, energy storage arises from the accumulation of electronic and ionic charges at the interface between the electrode material (carbon) and the electrolyte solution, whereas in pseudocapacitors, faradic reactions of the electroactive species take place on the surface of electrode such as metal oxides.[3] Such charge storage mechanism requires high surface area.

The material and structure of the electrode play a key role in the development of high performance supercapacitor with improved power density, energy density, rate capability and cycle stability. Carbon materials with large surface area such as activated carbon, carbon fibers, carbon aerogels and carbon papers have been widely used as electrode materials for EDLCs.[4-9] The ideal properties of carbon as the electroactive material should include: (i) highly accessible electrochemical active surface area for electrolytes, (ii) good intra-and inter-particle electrical conductivity in porous network, (iii) good electrolyte accessibility to the intra-and inter-pore space of carbon materials, (iv) a hierarchically porous structure with interconnected channels for facilitating the rapid diffusion of ions at a high rate and (v) better electrochemical and mechanical stability for good cycling performance.[10] However, at high current density the electrochemical performance of EDLCs suffers from severe reduction due to the electrolyte accessible surface area, and the power capacity is usually limited by the electrode kinetic constraints, such as inner-pore ion transport,[11,12] which greatly hinders its practical application.

Activated carbon (AC) has earned its status as an electrode material in EDLCs due to its cost effectiveness and the large specific surface area and its ability to accumulate a large number of charges. However, the narrow pore size distribution in the range of micropores (<2 nm) makes it difficult for electrolyte ions to access the narrow inner pore space. Hence, an undesired decrease in capacitance is evident at high current density due to the resistance to the diffusion and transport of electrolyte ions through narrow inner-pores[13] and consequently, high rate performance can not be realized, which is important for high power supercapacitors. All the factors mentioned above may affect the electrolyte

*Department of Advanced Materials Chemistry, Korea University, 2511 Sejong-ro, Sejong 339-700, Republic of Korea.
Fax: +82-44-860-1331; Tel: + 82- 44-860-1494;
E-mail: jsyu212@korea.ac.kr

accessibility and the rapid ion diffusion, and thus limit the capacitance. Recently, graphene has attracted great interest for EDLCs.[14,15] As a two-dimensional (2D) carbon nanostructure, graphene can potentially combine the advantages of providing a fully accessible high specific surface area and high conductivity. However, a key issue is to avoid the restacking of the 2D sheets during electrode preparation, which is quite challenging.

Hierarchically porous carbon materials are widely used for energy storage due to their ability to reduce the resistance of electrolyte diffusion.[16-23] Hierarchically porous carbon materials, particularly mesopores in combination with macropores/micropores structures have enhanced properties compared with single-sized pore materials. This is due to the improved ionic transport through the larger pores of material and maintenance of a specific surface area on the level of fine pore system through micropores/mesopores.[24,25] Despite such promissing potential, it is challenging, to synthesize hierarchically nanostructured carbon materials with large uniform mesopore-size, which enable the ions to enter the mesopores more easily at a high current density.

Hierarchical nanostructured porous carbon having high specific surface area and 3D interconnected pore arrangement can facilitate efficient mass transport,[26] and thus is expected to display great performance as EDLC electrodes at high current density.[27] In recent years, hierarchical nanostructured carbon materials as electrode for EDLC have been reported in organic electrolytes [17,28-31] or in aqueous electrolyte in three-electrode system.[10-12,17,19] However, there are only few reports on hierarchical nanostructured carbon materials for EDLC using aqueous electrolyte in two-electrode system. Chen *et al.*[32] have synthesized mesoporous hollow carbon spheres by CVD method with the specific capacitance of 99 F g^{-1} using two-electrode system in aqueous electrolyte. Frackowiak and his group[33] reported the high specific capacitance of 191 F g^{-1} for mesoporous carbons prepared by an inverse replica technique. Guterl *et al.*[34] prepared ordered porous carbon by template method and reported the specific capacitance of 208 F g^{-1}.

In this work, we report a simple template synthesis of ordered multimodal porous carbon (OMPC) with hierarchical nanostructures including a macropore of 400 nm and mesopore of 21 nm in diameter. The as-synthesized OMPC possesses not only high surface area of 1161 m^2 g^{-1}, but also a well-developed 3D hierarchical nanostructure composed of macro-, meso- and micropores. This unique structure provides a more favorable path for penetration and transportation of electrolyte ions, demonstrating excellent supercapacitor performance of the OMPC especially at high current density.

2. Experimental

2.1 Materials

All chemicals were of analytical grade. Polystyrene (PS), phenol and paraformaldehyde (PFA) were purchased from Sigma-Aldrich. All chemicals were used as received without any further purification.Activated carbon was purchased from SAMCHUN Pure Chemical Co., South Korea.

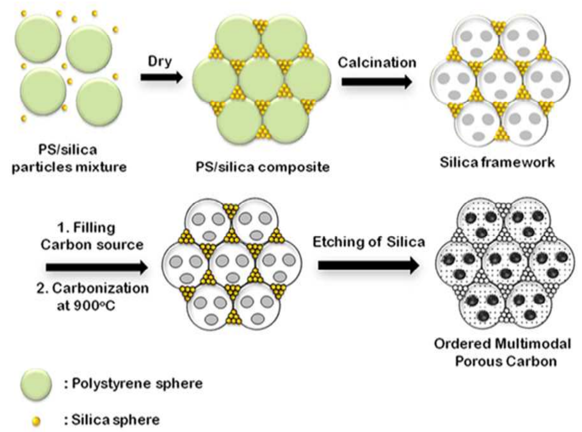

Fig. 1 Schematic representation for the fabrication of OMPC with hierarchical porosity.

2.2 Synthesis of ordered multimodal porous carbon (OMPC)

The synthesis method of the 3D interconnected ordered multimodal porous carbon (OMPC) is adapted from our previous work[35] and briefly described by the process shown in Fig. 1. Ordered hierarchical nanostructured silica (OHNS) was first synthesized using monodisperse polystyrene (PS) spheres as a template along with colloidal dispersion of small silica particles as described below. Initially, monodisperse PS spheres with 450 nm in size were mixed with a colloidal dispersion of much smaller silica particles with ca. 20 nm in size in the mass ratio of 100:1 for PS and silica particles, respectively. Upon gradual drying of the mixture, the monodisperse PS spheres self-assembled into an ordered lattice where the meso-sized smaller silica particles are forced to pack closely at the interstices between the PS spheres, which leads to the generation of particulate silica gels around the ordered PS lattice. Subsequently, the resulting composite was slowly heated to 550 °C and kept for 6 h under air to remove the PS colloids and to sinter the silica nanoparticles at their contact points, which results in firm ordered hierarchical nanostructured silica (OHNS) composed of particulate silica gels in the wall of the ordered macropore array. Interestingly, the voids between the sintered silica particles in the resulting OHNS also provide fully interconnected mesopores.[26] The as-synthesized OHNS framework was then used as a template for the synthesis of OMPC. 0.374 g of phenol was incorporated into the interstitial mesopore voids between the silica particles of 1.0 g of template by heating at 100 °C for 12 h under vacuum. The resulting phenol-incorporated OHNS template was then reacted with 0.238 g of PFA evaporated under vacuum at 130 °C for 24 h for polymerization to generate a phenol-resin/OHNS composite. After carbonization of the composite at 900 °C for 5 h and the etching of silica by 2.0 M of NaOH from the carbon/OHNS composite, OMPC was produced. The etching of meso-sized silica nanoprticles in the carbon/OHNS composite leaves corresponding mesopores in the cabon framework in additon to macropores formed by removal of PS spheres, resulting in OMPC with macro-, meso- and micropores in the carbon framework.

2.3 Instrumental analysis

X-ray diffraction (XRD) analysis was performed on a Rigaku Smartlab X-ray diffractometer with Cu Kα radiation (λ=1.5406 Å) operating at 40 kV and 30 mA. Scanning electron microscopy (SEM) analysis was carried out with a Hitachi (S-4700, Hitachi, Japan) microscope operated at acceleration voltage of 10 kV. Transmission electron microscopy (TEM) images were collected using JEOL FE 2010 microscope operated at 200 kV. N_2 sorption isotherms were measured on Micromeritics ASAP 2020 surface area and porosity analyser at 77 K. Before measurements, the samples were degassed at 150 °C at 20 mTorr pressure for 12 h. The specific surface areas (S_{BET}) were determined from nitrogen adsorption using the Brunauere-Emmette-Teller (BET) equation. The total pore volume (V_{total}) was determined from the amount of gas adsorbed at the relative pressure of 0.99, while the mesopore volume (V_{meso}) and micropore volume (V_{micro}) of the porous carbons were calculated from analysis of the adsorption isotherms using the Horvath–Kawazoe (HK) method. The pore size distribution (PSD) was calculated from the analysis of the adsorption branch using the Barrett-Joyner-Halenda (BJH) method.

2.4 Electrode fabrication and electrochemical characterization

The electrodes were prepared by mixing 75 wt % OMPC as an active material, 15 wt % super P, 10 wt % polyvinylidene fluoride (PVdF) and few drops of N-methylpyrrolidinone (NMP) as a solvent, which was added to form uniform slurry. The resulting uniform slurry was then coated onto graphite substrate serving as a current collector. The addition of super P content facilitates electron transport from the active materials to the current collector.[36] The native carbon not only improves the local conductivity but also prevents the detachment and aggregation of the active material during cycling.[37]The electrode area and mass of active material were 1.0 cm^2 and 1.5 mg, respectively. The coated electrodes were dried at 80 °C overnight in vacuum oven. The electrochemical performances of the electrodes were characterized by cyclic voltammetry (CV), galvanostatic charge/discharge (GCD) measurements and electrochemical impedance spectroscopy (EIS). The commercially available activated carbon was also studied under the same electrochemical conditions for the comparison.

The electrochemical properties of the supercapacitor electrodes were tested in aqueous electrolyte (1.0 M H_2SO_4) using a two-electrode system. The cycling range was 0.0 to 1.0 V at various scan rate of 10-100 mVs^{-1}. The galvanostatic charge/discharge properties were measured in the potential range of 0.0 to 1.0 V at the different current densities of 0.5, 1, 3, 5 and 10 A g^{-1}, respectively. All the electrochemical measurements were carried out with electrochemical workstation (Biologic VMP3). The EIS measurements were carried out at Biologic VSP electrochemical workstation in the frequency range from 10 kHz to 10 mHz with amplitude of superimposed AC signal of 10 mV.

3. Results and Discussion

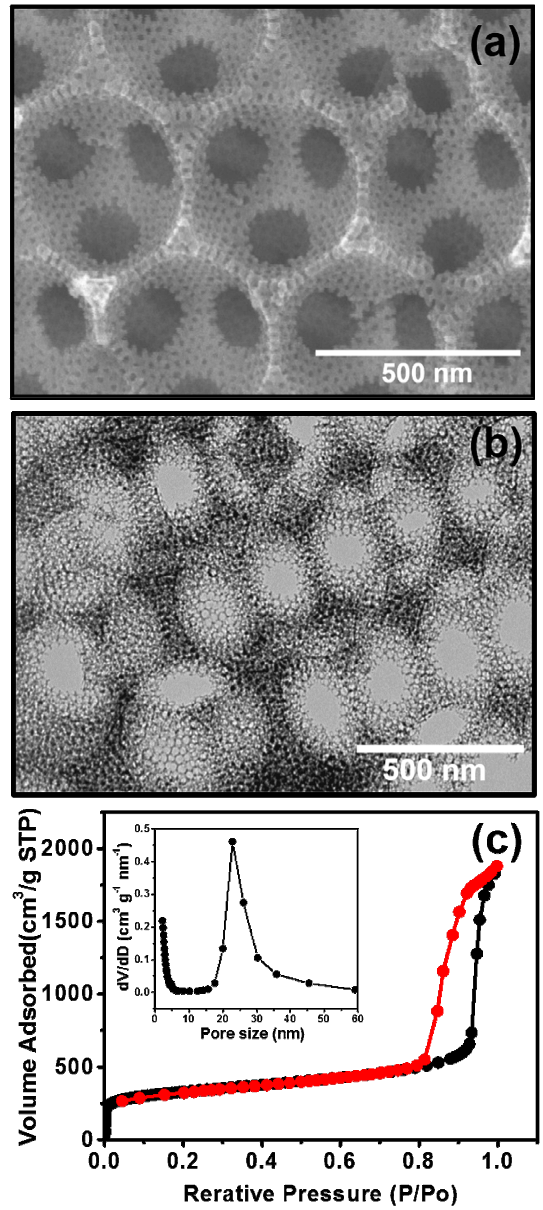

Fig. 2 (a) SEM, (b) TEM images and (C) N_2 adsorption-desorption isotherms, and inset shows pore size distribution curve of OMPC material.

The SEM and TEM images showing the morphology of as-synthesized OMPC sample are shown in Fig.2(a) and (b). It reveals that OMPC sample has a unique multimodal porous carbon framework with highly ordered hierarchical nanostructure. The macropores of OMPC sample are arranged in highly ordered hexagonal array with the macropores of ca. 400 nm in diameter, which are interconnected to each other with small connecting pores. The mesopores with ca. 20 nm in size are also interconnected to each other, embedded in the bigger macropore wall and open to the macropore wall. Fig. 2(a) clearly shows that the pores of the OMPC are uniform, closely-packed and roughly spherical with highly ordered hierarchical nanostructure.

Fig. 2(c) shows nitrogen sorption isotherm of the OMPC, which represents type IV with a H2 hysteresis loop (IUPAC nomenclature classification),[38] and is similar to typical isotherm patterns of mesoporous adsorbents. N_2 adsorption at a lower relative pressure of < 0.1 P/P_0, suggests the presence of micropores in synthesized OMPC, indicating that the OMPC material has micropores as well mesopores and macropores. The pore size distribution is centered at ca. 21 ± 3 nm, which is highly consistent with that observed from the SEM and TEM images. The OMPC exhibits a large BET surface area (S_{BET}) of 1161 m^2 g^{-1} and a total pore volume (V_{total}) of 2.78 cm^3 g^{-1}, which are mainly attributed to the presence of the mesopores (2 nm < pore size < 50 nm) in the framework. The mesopore volume (V_{meso}) is 2.53 cm^3 g^{-1}, representing ca. 87 % of the total pore volume. The textural parameters of the OMPC are summarized in Table 1. BET surface area of OMPC is higher than recently reported ordered mersoporous carbon (687 m^2 g^{-1}),[39] mesoporous carbon decorated with graphene (903 m^2 g^{-1}),[40] and template-fabricated three-dimensional ordered mesoporous carbon (601 m^2 g^{-1}).[29] Compared to commercial activated carbon (AC) which has a BET surface area of 851 m^2 g^{-1} (Fig. S1 of elelctronic supplementary inforamtion (ESI)), as-synthesized OMPC material possesses higher surface area along with higher mesoporosity.

Table 1 Textural properties of OMPC and AC.

Sample	S_{BET} (m^2 g^{-1})	V_{micro} (cm^3 g^{-1})	V_{meso} (cm^3 g^{-1})	V_{total} (cm^3 g^{-1})	Pore size (nm)
OMPC	1161.6	0.25	2.53	2.78	21 ± 3
AC	851.0	0.37	0.18	0.55	~ 2

S_{BET}: BET surface area, V_{micro}: micropore volume, V_{meso}: mesopore volume calculated by the t-plot method, V_{total}: total pore volume.

High specific surface area along with the unique ordered hierarchical nanostructure composed of a well-developed 3D interconnected ordered macropore framework with open mesopores embedded in the macropore walls of the OMPC material is favorable for improving both the pseudocapacitance and the electric double-layer capacitance because of the easily accessible hydrated ions in the electrolyte to the exterior and interior pore surfaces.[41,42]

The electrochemical performance of OMPC as a electrode material was examined by cyclic voltammetry (CV), galvanostatic charge-discharge (CD) measurement and electrochemical impedance spectroscopy (EIS) in aqueous electrolyte of 1.0 M H_2SO_4. Fig. 3(a) represents the CV of the OMPC and AC electrode at 10 mV s^{-1}. An ideal rectangular CV curve is obtained for OMPC, that exhibits typical characteristic of EDLC with a good charge propogation and easy ion transport in the electrode materials. It is noted that capacitive current arising from OMPC electrode is much higher than that of AC electrode at the same scan rate, suggesting that unique ordered hierarchical nanostructure of OMPC electrode has much higher specific capacitance.[43] Fig. 3(b) represents the CV curves of the OMPC sample recorded at different scan rates (10-100 mV s^{-1}). The rectangular symmetry in all CV curves of OMPC electrode can be

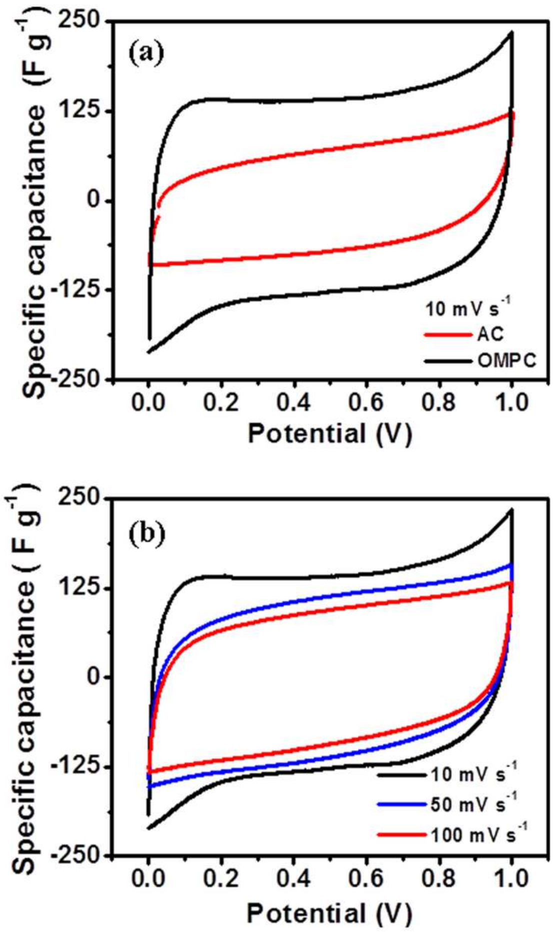

Fig. 3 (a) Cyclic voltammogram profiles of the electrodes made from AC and OMPC and (b) cyclic voltammogram profiles of the electrode made from OMPC at different scan rates in 1.0 M H_2SO_4 electrolyte.

certainly maintained without drastic changes even at a high scan rate of 100 mV s^{-1} which can be attributed to the hierarchical meso- and macroporous architectures of OMPC sample, which retains the good capacitive behavior even at higher scan rate. In addition, combined hierarchical micropores/mesopores are beneficial for fast ionic transportation within the mesopores and diffusion from mesopores to micropores.[44]

The electrochemical performance of the unique ordered hierarchical nanostructue of OMPC as a electrode material was further evaluated by CV and galvanostatic CD measurements. The specific capacitance (F g^{-1}) was calculated by the following equation (1):[45]

$$C_s = 2 \times \frac{I}{m \times {}^{dV}\!/_{dt}} \quad (1)$$

where C_s is the specific capacitance, I is the applied current, m is the mass of the each electrode material, and dV/dt is the potential scan rate in CV measurements and slope of the discharge curve in CD measurements, respectively. The factor

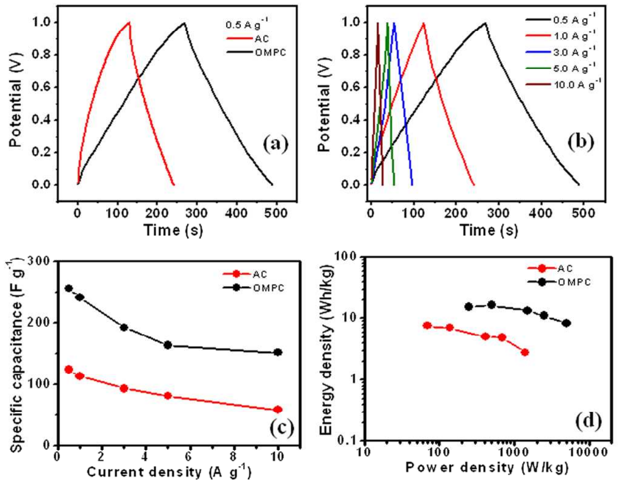

Fig. 4 (a) Galvanostatic charge-discharge curves of the electrodes made from AC and OMPC, (b) galvanostatic charge-discharge curves of the OMPC electrode at different current densities in 1.0 M H_2SO_4, (c) variation in specific capacitance of AC and OMPC electrodes as a function of current density and (d) Ragone plot of AC and OMPC electrodes.

of 2 is used because the series capacitance is formed in a two-electrode system.[45]

Fig. 4(a) represents the galvanostatic CD curves of OMPC and AC electrodes at a current density of 0.5 A g^{-1}.The smaller IR drop suggests a smaller internal resistance of OMPC electrode compared to the AC electrode. It is clearly observed that OMPC electrode shows significantly longer CD time, indicating higher specific capacitance (257 F g^{-1}) than AC (123 F g^{-1}) electrode at lower current density of 0.5 A g^{-1}. These results are in good agreement with CV results in Fig. 3. Li et al.[16] synthesized mesoporous carbon spheres with a hierarchical form-like pore structure for electrochemical capacitors, and a specific capacitance of 208 F g^{-1} at the current density of 0.5 A g^{-1} in 2.0 M H_2SO_4 aqueous solution was obtained. Chen et al.[32] have synthesized mesoporous hollow carbon spheres by CVD method with the specific capacitance of 99 F g^{-1} at 0.2 A g^{-1}. Mesoporous carbons prepared by an inverse replica technique yielded the specific capacitance of 191 and 161 F g^{-1} at 1.0 A g^{-1} for two different mesoporous carbon structures in 1.0 M H_2SO_4 electrolyte.[33] Ordered porous carbon synthesized from template method using sucrose as carbon source showed the specific capacitance of 208 F g^{-1} at 0.2 A g^{-1} in aqueous solution of 1 M H_2SO_4.[34] Li et al.[46] have shown that mesoporous carbon spheres prepared by facile polymerization-induced colloid aggregation method provided the specific capacitance of 211 F g^{-1} in 5.0 M H_2SO_4.

To further evaluate the rate capabilities of the OMPC electrode, the galvanostatic CD curves at different current densities of 0.5 to 10 A g^{-1} were recorded and shown in Fig. 4(b). All the CD curves show isosceles triangular shapes with very small ohmic drop, suggesting good coulombic efficiency and excellent capacitive behavior. The specific capacitances obtained for OMPC electrode at 0.5, 1.0, 3.0, 5.0 and 10.0 A g^{-1} are 257, 242, 193, 164 and 152 F g^{-1}, respectively. It can be clearly seen that the capacitance of OMPC electrode decays slowly with the increase of current density, suggesting a good rate capability. Its capacitance at a high current density of 5.0 A g^{-1} is as high as 164 F g^{-1}, 64 % of 257 F g^{-1} at 0.5 A g^{-1}, and it still keeps 60 % of the initial capacitance even at 10.0 A g^{-1} (152 F g^{-1}). On the other hand, the capacitance of AC electrode decreases to 59 F g^{-1} at 10 A g^{-1}, 48 % of the initial value at 0.5 A g^{-1} as shown in Fig 4(c).

The better rate capability is mainly attributed to the macroporous architectures in the OMPC sample. Although the macoropore size does not have a significant effect on the rate capability of carbon, but the interconnection of macropores plays an important role in the charge-discharge process, since the macropores can keep a large amount of electrolyte, and their interconnection gives an easy ion transport path from the bulk electrolyte to mesopores and microspores which enhance the rate performance and utilization of micropores.

The specific energy (SE) and power (SP) densities are critical performance indices for ECs, which can be calculated at different current densities using the following equations:[45]

$$E(\mathrm{Whkg^{-1}}) = \frac{1}{2} C_s \Delta V^2 \times \frac{1000}{3600} \quad (2)$$

$$\mathrm{P(Wkg^{-1})} = \frac{E}{t} = \frac{I\Delta V}{2m} \times 1000 \quad (3)$$

where E is the specific energy density, C_s is the specific capacitance, ΔV is the potential range, P is power density and t is the time of discharge.

Fig. 4(d) shows the Ragone plot of the OMPC and AC electrodes at different current densities. For both the electrodes, as the power density increases, energy density decreases but the rate of decrement of AC is much faster compare to OMPC electrode. The superior performance of the OMPC is highlighted by the excellent energy density retention over the whole power density investigation region. As shown in Fig. 4(d), as the power density increases from 0.25 to 5.0 kW kg^{-1}, the energy density decreases slowly from 15 to 8 Wh kg^{-1} for OMPC electrode. In contrast, as the power density increases from 0.069 to 1.3 kW kg^{-1}, the energy density decreases quickly from 7 to 2 Wh kg^{-1} for AC electrode. Based on the above results, we can say that the OMPC electrode is capable of delivering high power without profound loss in energy, indicating a promising application in electrochemical capacitors. The result of OMPC material is comparable to PS-based hierarchical porous carbon material[19] and is better than those obtained from hierarchical structures containing mesoporous carbon sphere-graphene oxide sheet[47] and mesoporous carbon nanofiber arrays.[48] The excellent rate performance of OMPC electrode benefits from its high specific surface area and unique ordered hierarchical nanostructure which favors the rapid charge propogation within the electrode and enables the easy access of the electrolyte ions to the surface of carbon and mesopores of OMPC to form EDLC. In contrast, predominent small micropores and poor interconnectivity of pores of AC (Fig. S2 of ESI) with lack of 3D interconnected ordered hierachical porosity observed in the OMPC result in less efficient mass

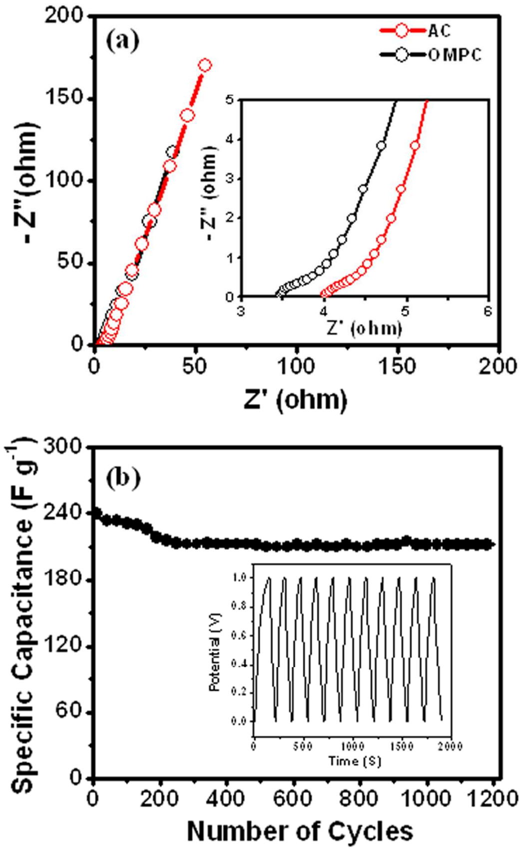

Fig. 5 (a) Nyquist impedance plots of the electrodes made from AC and OMPC in 1.0 M H_2SO_4 electrolyte. Inset shows the high-frequency region and (b) cycle stability of the OMPC electrode at the current density of 1.0 A g^{-1}. Inset shows the galvanostatic charge-discharge curves of first 10 cycles.

transport, which validates the importance of hierarchical nanostructure composed of macro-, meso- and micropores for the improvement of electrochemical perfromance like in OMPC.

The Nyquist impedance spectra of the OMPC and AC electrodes are shown in Fig. 5(a). It is observed that both the plots exhibit a semicircle in the high frequency range and a sloped line in the low frequency range. The point intersecting at the real axis in the high frequency range is the internal resistance (R_s) of the electrode material, which includes the total resistances of the ionic resistance of the electrolyte, the intrinsic resistance of active materials, and the contact resistance at the active material/current collector interface.[49] The semicircle at high frequency region indicates the influence of material porosity and thickness on the migration rate of the ions from the electrolyte inside the porous carbons,[50] and the diameter of the semicircle is a measure of charge transfer resistance, R_{ct} and is associated with the surface area and electrolyte conductivity within the pores of electrode materials.[19] Generally, a small value of diameter of the semicircle indicates a high ion transfer/diffusion rate into the pores of electrode materials.[51] The R_s of OMPC and AC electrodes was measured to be 3.46 and 4.01 Ω, respectively, while R_{ct} was approximated to be 0.20 and 0.31 Ω, respectively. Both the R_s and R_{ct} of the AC electrode are higher than those of the OMPC electrode. The significant difference in pore structure between OMPC and AC electrodes clearly demonstrates the excellent ion diffusion ability of the OMPC resulting from the hierarchical nanostructure.

The cycle stability of supercapacitors is a crucial parameter for their practical applications. The electrochemical stability of OMPC sample as an electrode material for supercapacitor is evaluated by galvanostatic CD cycles at the current density of 1.0 A g^{-1} for 1200 cycles. The variation of specific capacitance, C_s as a function of cycle number is shown in Fig. 5(b). The CD profiles exhibited an isosceles triangular shape (inset of Fig. 5(b)), which is the characteristic of the double layer charge storage mechanism. The initial specific capacitance of the OMPC electrode is 240 F g^{-1} which decreases and remains stable at 216 F g^{-1} after 1200 cycles. The specific capacitance shows slight decrease for the first 200 cycles and then remaines stable with increasing cycle number. About 90 % of the intial specific capacitance is preserved after 1200 galvanostatic CD cycles, indicating the excellent electrochemical cycling stability of OMPC electrode, which has high potential for long-term applications.

The high performance of OMPC can be attributed to the 3D hierarchical nanostructure that plays a very important role in the formation of double-layer capacitance and to their unique hierarchical porous structures that favors the fast diffusion of electrolyte ions into the pores.[11] The hierarchical porous structure design is based on the different behaviors of electrolyte in pores with different sizes. Electrolyte in macropores, which maintains its bulk phase behavior, can reduce the transport length of ions inside a porous framework. Electrolyte ions have a smaller probability to crash against pore walls of large mesopores and hence reduce ion transport resistance. Ion-buffering reservoirs can be formed in the macropores to minimize the diffusion distances to the interior surfaces. Furthermore, the mesoporous walls provide low-resistant pathways for the ions through the porous framework, and the micropores strengthen the electric-double-layer capacitance.[30] Therefore, a combination of macro-, meso-, and micropores as found in our OMPC can result in high-performance electrode materials with short ion transport distance, low resistance, and large charge storage density.[52]

4. Conclusions

The as-synthesized OMPC possesses not only high surface area, but also a unique 3D interconnected hierarchical porosities composed of macro-, meso-, and micropores, which enable OMPC to store and release large electrical charges efficiently whether at a low-mid or high rate. The well-developed 3D interconnected ordered macroporous framework along with open mesopores embedded in the macropore walls favor fast mass transport at high charge-discharge rates, providing better EDLC performance. The OMPC electrode exhibits a highest capacitance of 257 F g^{-1} at low current density of 0.5 A g^{-1} and 152 F g^{-1} at high current density of 10 A g^{-1} in aqueous electrolyte of 1.0 M H_2SO_4. This hierarchical nanostructure of OMPC can deliver energy density of 8.4 Wh kg^{-1} at a power density of 5.0 kW kg^{-1}, and about 90 % of specific capacitance is preserved after 1200 galvanostatic CD cycles, indicating the excellent electrochemical cycling stability of OMPC electrode. These results reveal that OMPC possesses better electrochemical performance compared to commonly used electrode materials such as AC which makes OMPC a potential candidate for supercapacitor application.

Acknowledgements

This work was supported by Korea University (2014). Authors also would like to thank the Korean Basic Science Institute at Jeonju, Daejeon and Pusan for SEM and TEM measurements.

Notes and references

Department of Advanced Materials Chemistry, Korea University, 2511 Sejong-ro, Sejong 339-700, Republic of Korea. Fax: +82-44-860-1331; Tel: + 82- 44-860-1494; E-mail: jsyu212@korea.ac.kr

† Electronic Supplementary Information (ESI) available: BET, SEM and TEM images of activated carbon (AC). See DOI: 10.1039/b000000x/

1 P. Simon and Y. Gogotsi, *Nat. Mater.*, 2008, **7**, 845.
2 M. Winter and R. J. Brodd, *Chem. Rev.*, 2004, **104**, 4245.
3 S. Chaudhari, D. Bhattacharjya and J.-S. Yu, *RSC Adv.*, 2013, **3**, 25120.
4 Y. Zhai, Y. Dou, D. Zhao, P. F. Fulvio, R. T. Mayes and S. Dai, *Adv. Mater.*, 2011, **23**, 4828.
5 L. Zhao, L.-Z. Fan, M. -Q. Zhou, H. Guan, S. Qiao, M. Antonietti and M.-M. Titirici, *Adv. Mater.*, 2010, **22**, 5202.
6 J. Xue, C. Henry, J. Lee and B. D. Vogt, *RSC Adv.*, 2014, **4**, 3675.
7 Z. Zhou, X.-F. Wu and H. Hou, *RSC Adv.,* 2014, **4**, 23622.
8 R. Madhu, K. V. Sankar, S.-M. Chen and R. K. Selvan, *RSC Adv.,* 2014,**4**, 1225.
9 Y. Ren, J. Zhang, Q. Xu, Z. Chen, D. Yang, B. Wang and Z.Jiang, *RSC Adv.,* 2014,**4**, 23412.
10T.-C.Chou, C.-H. Huang, R-A Doong and C.-C. Hu, *J. Mater. Chem. A,* 2013, **1**, 2886.
11 D. W. Wang, F. Li, M. Liu, G. Q. Lu and H. M. Cheng, *Angew. Chem. Int. Ed.*, 2008, **47**, 373.
12 D. W. Wang, F. Li, H. T. Fang, M. Liu, G. Q. Lu and H. M. Cheng, *J. Phys. Chem. B*, 2006, **110**, 8570.
13 E. Frackowiak and F. Beguin, *Carbon*, 2001, **39**, 937.
14 A. K. Geim and K. S. Novoselov, *Nat. Mater.*,2007, **6**,183.
15 L. L. Zhang, R. Zhou and X. S. Zhao, *J. Mater. Chem.*,2010, **20**, 5983.
16 F. J. Li, M. Morris and K. Y. Chan, *J. Mater. Chem.*,2011, **21**, 8880.
17 Q. Li, R. R. Jiang, Y. Q. Dou, Z. X. Wu, T. Huang, D. Feng, J.P. Yang, A. S. Yu and D.Y.Zhao, *Carbon*, 2011, **49**,1248.
18 Z. L. Xie, R. J. White, J. Weber, A. Taubert and M. M. Titirici, J. *Mater. Chem.*, 2011, **21**, 7434.
19 F. Xu, R. J. Cai, Q. C. Zeng, C. Zou, D. C. Wu, F. Li, X. E. Lu,Y. R. Liang and R. W. Fu, *J. Mater. Chem.*,2011, **21**, 1970.
20 H. A. Xu, Q. M. Gao, H. L. Guo and H. L. Wang, *Microporous Mesoporous Mater.*, 2010, **133**, 106.
21 S. Y. Yang, K. H. Chang, H. W. Tien, Y. F. Lee, S. M. Li, Y. S. Wang, J. Y. Wang, C. C. M. Ma and C. C. Hu, *J. Mater. Chem.*,2011, **21**, 2374.
22 S. Q. Fan, B. Fang, J. H. Kim, B. Jeong, C. Kim, J.-S. Yu and J. Ko, *Langmuir*, 2010, **26**, 13644.
23 B. Fang, M. S. Kim, J. H. Kim, S. Lim and J. -S. Yu, *J. Mater. Chem.*, 2010, *20*,10253.
24 Z. Y. Yuan and B. L. Su, J. Mater. Chem.,2006, 16, 663.
25 Y. S. Hu, P. Adelhelm, B. M. Smarsly, S. Hore, M. Antonietti and J. Maier, *Adv. Funct. Mater.*, 2007, **17**, 1873.
26 G. Chai, I.Shin and J. -S. Yu, *Adv. Mater.,* 2004,**16**, 2057.
27 L. Zhang, S. Li, J. Zhang, P. Guo, J. Zheng and X. Zhao, *Chem. Mater.*, 2010, **22**, 1195.
28 S. Woo, K. Dokko, H. Nakano and K. Kanamura, *J. Mater. Chem.*,2008, **18**, 1674.
29 H.-J. Liu,W.-J. Cui,L.-H. Jin, C.-X.Wang and Y.-Y. Xia, *J. Mater. Chem.*, 2009, **19**,3661.
30 J. Chmiola, G. Yushin, Y. Gogotsi, C. Portet, P. Simon and P. L. Taberna, *Science*, 2006, **313**, 1760.
31 B. Fang, A. Bonakdarpour, M.-S. Kim, J.H. Kim, D. P. Wilkinson and J.-S. Yu, *Micropor. Mesopor. Mater.*, 2013, **244**, 799.
32 X. Chen, K. Kierzek, K. Cendrowski, I. Pelech, X. Zhao,J. Feng, R. J. Kalenczuk, T. Tang and E. Mijowska, *Colloids and Surfaces A: Physicochem. Eng. Aspects*,2012, **396**, 246.
33 A. B. Fuertes, G. Lota, T.A. Centeno and E. Frackowiak, *Electrochim. Acta*, 2005, **50**, 2799.
34 C. V.-Guterl, S. Saadallah, K. Jurewicz, E. Frackowiak, M. Reda, J. Parmentier , J. Patarin and F. Beguin, *Mater. Sci. Eng. B*, 2008, **108**, 148.
35 B. Fang, J. H. Kim. M.-S. Kim and J.-S. Yu, *Chem. Mater.*, 2009, **21**, 789.
36 B. Kang and G. Ceder, *Nature*, 2009, **458**,190.
37 S.-L. Jin, H. Deng, D. Long, X. Liu, L. Zhan, X. Liang, W. Qiao and L. Ling, *J. Power Sources*, 2011, **196**, 3887.
38 F. Rouquerol, J. Rouquerol and K. Sing, Adsorption by Powders and Porous Solids: Principles, Methodology and Applications, Academic Press, London, 1999.
39 X. Wang, C.-G. Liu, D. Neff, P. F. Fulvio, R. T. Mayes, A. Zhamu, Q. Fang, G. Chen, H. M. Meyer, B.Z. Jang and S. Dai, *J. Mater. Chem. A,* 2013, **1**,7920.
40 M. Li, J. Ding and J. Xue, *J. Mater. Chem. A*, 2013, **1**, 7469.
41 Y. C. Xing, *J. Phys. Chem. B*, 2004,**108**, 19255.
42 N. Timothy, A. Carlos, H. Bernadette, L. Ping, S. Nelson, A Andrea, F. Thomas, J. Timothy R. David and L. Dale, *J. Phys. Chem. C*, 2009, **113**, 19812.
43 R. K. Sharma, H. S. Oh, Y. G. Shul and H. S. Kim, *J. Power Sources*, 2007, **173**, 1024.
44 Y. W. Zhu, S. Murali, M. D. Stoller, K. J. Ganesh, W. W. Cai, P. J. Ferreira, A. Pirkle, R. M. Wallace, K. A. Cychosz, M. Thommes, D. Su, E. A. Stach and R. S. Ruoff, *Science*, 2011, **332**, 1537.
45 C.-C. Xiang, M. Li, M. Zhi, A. Manivannan and N. Wu, *J. Mater. Chem.*, 2012, **22**,19161.
46 W. Li, D. Chen, Z. Li, Y. Shi, Y. Wan, J. Huang, J. Yang, D. Zhao and Z. Jiang, *Electrohem. Commun.*, 2007, **9**, 569.
47 Z. B. Lei, N. Christov and X. S. Zhao, *Energy Environ. Sci.*, 2011,**4**, 1866.
48 E. Kang, G. Jeon and J. K. Kim, *Chem. Commun.*, 2013, **49**, 6406.
49 J.-W.Lang, X.-B.Yan, X. -Y. Yuan, J. Yang and Q.-J. Xue, *J. Power Sources*, 2011, **196**, 10472
50 M. Itagaki, Y. Hatada, I. Shitanda and K. Watanabe, *Electrochim. Acta*, 2010, **55**,6255.
51 C. L. Liu, W. S. Dong, G. P. Cao, J. R. Song, L. Liu and Y. S. Yang, *J. Electrochem. Soc.*,2008, **155**, F1.
52. B. Fang, J. H. Kim, M.-S. Kim and J.-S. Yu, *Accounts. Chem. Res.*, 2013, **46**, 1397.